Earth and Planetary Science Letters 419 (2015) 178–186

Contents lists available at ScienceDirect

Earth and Planetary Science Letters

www.elsevier.com/locate/epsl

Transition to an oxygen-rich atmosphere with an extensive overshoot triggered by the Paleoproterozoic snowball Earth

Mariko Harada [a,*], Eiichi Tajika [b], Yasuhito Sekine [a]

[a] Department of Earth & Planetary Science, University of Tokyo, Bunkyo 113-0033, Japan
[b] Department of Complexity Science & Engineering, University of Tokyo, Kashiwa 277-8561, Japan

ARTICLE INFO

Article history:
Received 4 November 2014
Received in revised form 27 February 2015
Accepted 5 March 2015
Available online 30 March 2015
Editor: J. Lynch-Stieglitz

Keywords:
Paleoproterozoic
atmospheric oxygen
snowball Earth
the Great Oxidation Event
biogeochemical cycles

ABSTRACT

The Earth is thought to have multiple stable, steady-states regarding climate modes and atmospheric oxygen levels. The Paleoproterozoic is a remarkable period in Earth's history because of the simultaneous occurrence of large climatic and redox transitions between steady states; i.e., snowball Earth glaciation and the rise of oxygen. Geochemical evidence suggests that the oxygen rise was a dynamic transition with an extensive, long-term overshoot. However, previous models have not explained the dynamics of the oxygen rise, leaving its causal mechanism poorly understood. In the present study, we suggest that the oxygen transition with an overshoot occurred in response to a climatic transition at the termination of the snowball glaciation. Biogeochemical cycle modelling indicates that prolonged super-greenhouse conditions and effective nutrient input to the ocean after the glaciation lead to high levels of primary productivity and burial of organic carbon. This causes an abrupt jump of oxygen levels within $\sim 10^4$ yr after the glaciation and an extensive oxygen overshoot to the present atmospheric level. The overshoot persists for $\sim 10^8$ yr because net consumption of oxygen in the atmosphere–ocean system is inefficient. We show that the post-glacial jump of oxygen levels occurred in biologically short timescale, which may have stimulated the ecological shift and/or biological innovations toward the prosperity of oxygen-dependent life.

1. Introduction

Multiple lines of geological and geochemical evidence indicate that the oxygen (O_2) levels in Earth's atmosphere–ocean system shifted markedly and irreversibly from anoxic ($<10^{-5}$ of the Present Atmospheric Level, PAL) (Farquhar et al., 2007; Pavlov and Kasting, 2002) to oxic ($\sim 10^{-2}$ PAL) (Rye and Holland, 1998) during the Paleoproterozoic, i.e., 2.45–2.2 billion years ago (Ga) (although, the recent study suggests that the O_2 levels would have been as low as 10^{-3} PAL in the Mesoproterozoic; Planavsky et al., 2014). Previous studies propose that the drastic shift in Earth's redox state can be interpreted as a jump from low to high steady states of atmospheric O_2 levels (Claire et al., 2006; Goldblatt et al., 2006). Such an event-like unidirectional jump in O_2 levels might have been triggered simply by an increase in oxygen input from the biosphere (Goldblatt et al., 2006) or by a decrease in reductant input from Earth's interior (Claire et al., 2006; Gaillard et al., 2011; Goldblatt et al., 2006). However, recent geochemical data, e.g., the global deposition of sulfate minerals at 2.2–2.1 Ga (Bekker and Holland, 2012; Schröder et al., 2008) and the geochemical evidence of the global deep-water oxygenation in 2.1 Ga reported from in the Francevillian Group, the Republic of Gabon (Canfield et al., 2013), suggest that the oxidation would have been a dynamic transition of O_2 levels accompanying an intense overshoot lasting for $\sim 10^8$ yr, which is termed the Great Oxygen Transition (GOT) (Lyons et al., 2014). The O_2 levels might have reached around 0.1–1 PAL during this period (Bekker and Holland, 2012; Lyons et al., 2014). Such dynamic behavior of the GOT cannot be explained solely by the event-like O_2 jump proposed by previous studies (Claire et al., 2006; Gaillard et al., 2011; Goldblatt et al., 2006); instead, it appears to require strong oxidative forcing.

We propose here that deglaciation after the Paleoproterozoic snowball glaciation at 2.2 Ga (Evans et al., 1997; Kirschvink et al., 2000) triggered the GOT. Previous studies suggest that a long-term shutdown of atmosphere–ocean interactions during the snowball glaciation resulted in the accumulation of volcanic carbon dioxide

* Corresponding author at: Kiban Building, m.b. 408, Department of Earth & Planetary Science, University of Tokyo, 5-1-5 Kashiwanoha, Kashiwa, Chiba 277-8561, Japan. Tel. & fax: +81 4 7136 3954.
E-mail address: harada@astrobio.k.u-tokyo.ac.jp (M. Harada).

http://dx.doi.org/10.1016/j.epsl.2015.03.005
0012-821X/

(CO_2) in the atmosphere. Theoretical models show that the buildup of CO_2 to a level of ~0.7 atm at 2.2 Ga eventually caused a climate jump to an ice-free greenhouse state (Caldeira and Kasting, 1992; Tajika, 2003). Such a greenhouse climate during deglaciation should have induced a strong perturbation of the biogeochemical cycle.

The near-simultaneous occurrence of the snowball glaciation and the rise of oxygen suggest a close relationship between these two events (Claire et al., 2006; Kirschvink et al., 2000; Kopp et al., 2005; Lyons et al., 2014). Some geological studies suggest that the oxygenation was caused by the snowball glaciation (Kirschvink et al., 2000; Kopp et al., 2005). In the Transvaal Supergroup, South Africa, a massive deposition of manganese–iron oxides is found directly above a low-latitude glacial diamictites, which implies that the rise of O_2 might have occurred after the glaciation (Kirschvink et al., 2000; Kopp et al., 2005). The evidence of the deposition of sulfate minerals found above the manganese and iron formation (Schröder et al., 2008) suggests that the O_2 rise after the snowball glaciation was a massive and long-lasting event. However, temporal variations in the oxygenation and the achieved O_2 levels are poorly quantified. Quantification of the dynamics of the O_2 rise after the snowball glaciation and its comparison with geological records during the GOT are critical to understand the linkage between the Paleoproterozoic snowball glaciation and the GOT. In addition, knowledge on the timescales and magnitude of the environmental oxygenation is important because they would have determined the biological evolution or ecological shift that occurred in the Paleoproterozoic (El Albani et al., 2010; Payne et al., 2009).

In this study, we aim to discuss the linkage between the Paleoproterozoic snowball glaciation and the GOT. Using a biogeochemical cycle model, we examine biogeochemical responses in the atmosphere–ocean system to a climate jump at the termination of the snowball glaciation, and quantify the timescales and magnitude of the O_2 rise after the glaciation. In the next section (Section 2), we describe our numerical model, especially the parts that are essential and original in this study. Full model descriptions are in the Supplementary Materials. We then show the numerical results (Section 3), compare the results with geological records and discuss its implications for early life evolution (Section 4). Finally, we summarize this study (Section 5).

2. Methods

2.1. Model description and experimental design

Our model simulates the time evolution of climate, biogeochemical processes, and redox conditions in the atmosphere–ocean system after the snowball glaciation. The model consists of three boxes: atmosphere, surface ocean, and deep ocean (Fig. 1), where the abundances of gaseous molecules, such as CO_2, O_2, and CH_4 and/or dissolved species including dissolved inorganic carbon (DIC), alkalinity, phosphorous (PO_4), O_2, and calcium ion (Ca^{2+}) are calculated. These boxes exchange key elements through atmosphere–ocean interactions, biogeochemical reactions and ocean circulations. Removal of elements from the atmosphere–ocean system occurs through carbonate precipitation and organic carbon burial in the oceans as well as H_2 escape from the atmosphere to space, whereas supplies of elements take place via chemical weathering of the continents, reductant input and volcanic degassing from mantle (Fig. 1). Surface temperatures are calculated from atmospheric CO_2 concentration, which is obtained from the results from a radiative–convective climate model of Kasting and Ackerman (1986).

In the surface ocean, photosynthesis produces organic carbon, which is in turn exported to the deep ocean. In the deep ocean,

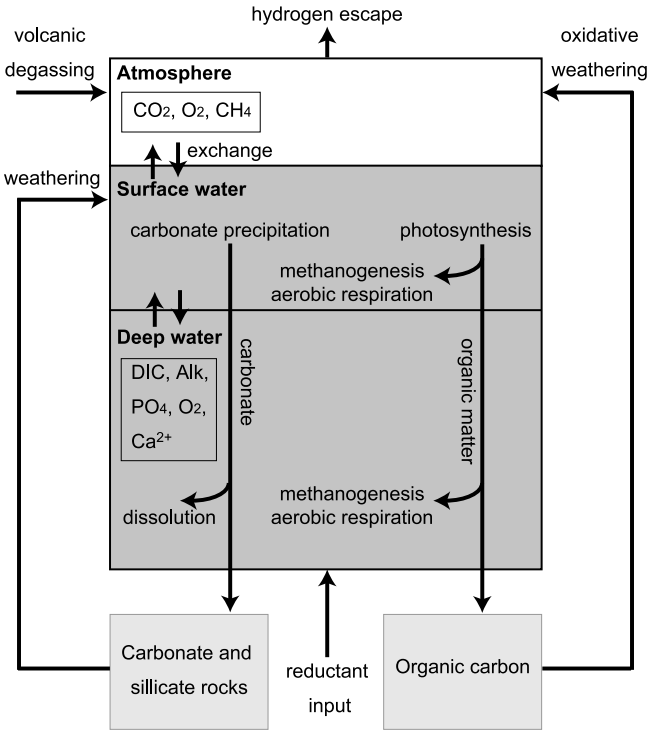

Fig. 1. Diagram of the biogeochemical cycle model. Atmosphere–ocean system are represented by three boxes i.e., atmosphere, surface ocean, and deep ocean. Arrows express exchange of key elements between boxes, as well as external inputs to and outputs from the atmosphere–ocean system. The equations concerning each flux are described in Section 2 and Supplementary Materials.

most of exported organic carbon is decomposed through aerobic respiration and methanogenesis. In the atmosphere, CH_4 produced by methanogenesis is finally oxidized by O_2, forming CO_2. Thus, the net production rate of O_2 in the atmosphere–ocean system corresponds to the rate of organic carbon burial in the ocean. We consider that the rate of organic carbon burial is proportional to the rate of export production and that the rate of export production is expressed as a function of phosphorus concentrations in the surface ocean (Yamanaka and Tajika, 1996) (also see Section 2.3). Phosphorus riverine input is considered to be proportional to the rate of chemical weathering of silicate and carbonate minerals in the continents (see Section 2.2). Accordingly, the biological production rate of O_2 is strongly affected by surface temperature. Indeed, it has been widely accepted that there are linkages in the Earth's system between global warming, an enhancement of nutrient supply via continental weathering, and an increase in oceanic biological productivity (e.g., oceanic anoxic events in the Phanerozoic) (e.g., Jenkyns, 2010). In our model, the chemical weathering rate is described as functions of both partial pressure of CO_2 and surface temperature, multiplied by the factor representing weathering efficiency (Berner, 1991; Tajika, 2003) (also see Section 2.2). The biological production of CH_4 occurs through decomposition of organic matter by methanogenesis.

Regarding the initial conditions, we set 0.7 atm of atmospheric CO_2 given that this level is required to end the snowball glaciation in the Paleoproterozoic (Tajika, 2003). Then, we explore the time evolution of each component in the atmosphere–ocean system after the snowball deglaciation. In sensitivity tests, we varied initial conditions, such as the atmospheric CO_2, oceanic phosphorus concentration and alkalinity, the parameters of weathering efficiency and phosphorous cycles in the oceans (Fig. 1 and Figs. S1–S5) (see Supplementary Materials for more details on the sensitivity tests).

Table 1
Mass balance equations, and their symbols and descriptions.

Symbol	Description	Mass balance equation (mol/yr)
$\mathbf{C}_{AS}$	Inorganic carbon in the atmosphere and surface ocean	$\frac{d\mathbf{C}_{AS}}{dt} = F_{vc} + F_{wo\_C} + F_{esc\_H} + F_{oxi\_M} + F_{wc} - F_{pc} - F_{po\_C} + F_{cir\_C}$
$\mathbf{C}_{D}$	Inorganic carbon in the deep ocean	$\frac{d\mathbf{C}_{D}}{dt} = F_{dc} + F_{dgD\_C} - F_{cir\_C}$
$\mathbf{O}_{AS}$	Oxygen (O_2) in the atmosphere and surface ocean	$\frac{d\mathbf{O}_{AS}}{dt} = F_{po\_O} - F_{wo\_O} - F_{oxi\_O} - F_{esc\_H} + F_{cir\_O}$
$\mathbf{O}_{D}$	O_2 in the deep ocean	$\frac{d\mathbf{O}_{D}}{dt} = -F_{cir\_O} - F_{dgD\_O}$
$\mathbf{M}_{AS}$	Methane (CH_4) in the atmosphere and surface ocean	$\frac{d\mathbf{M}_{AS}}{dt} = F_{dgS\_M} + F_{dgD\_M} + F_{wo\_M} - F_{oxi\_M} - F_{esc\_H}$
$\mathbf{Ca}_{S}$	Calcium ions (Ca^{2+}) in the surface ocean	$\frac{d\mathbf{Ca}_{S}}{dt} = F_{wc} + F_{ws} - F_{pc} + F_{cir\_Ca}$
$\mathbf{Ca}_{D}$	Calcium ions in the deep ocean	$\frac{d\mathbf{Ca}_{D}}{dt} = F_{dc} - F_{cir\_Ca}$
$\mathbf{P}_{S}$	Phosphorus ions (PO_4) in the surface ocean	$\frac{d\mathbf{P}_{S}}{dt} = F_{rp} - F_{po\_P} + F_{cir\_P}$
$\mathbf{P}_{D}$	Phosphorus ions in the deep ocean	$\frac{d\mathbf{P}_{D}}{dt} = F_{dgD\_P} - F_{cir\_P}$
$\mathbf{Alk}_{S}$	Alkalinity in the surface ocean	$\frac{d\mathbf{Alk}_{S}}{dt} = 2 \times (F_{wc} + F_{ws} - F_{pc} + F_{cir\_Ca})$
$\mathbf{Alk}_{D}$	Alkalinity in the deep ocean	$\frac{d\mathbf{Alk}_{D}}{dt} = 2 \times (F_{dc} - F_{cir\_Ca})$

Table 2
Symbols that are used to express fluxes between the boxes.

Symbol	Description
F_{vc}	volcanic degassing flux of CO_2
F_{red}	reductant (Fe^{2+}) input (= anoxygenic photosynthesis rate)
F_{wc}	weathering of carbonate rocks
F_{ws}	weathering of silicate rocks
F_{rp}	phosphorus river input
F_{wo}	amount organic carbon expose on land
F_{wo_M}	CH_4 produced by weathering of terrestrial organic matter
F_{wo_C}	CO_2 produced by weathering of terrestrial organic matter
F_{wo_O}	O_2 consumed by weathering of terrestrial organic matter
F_{pp}	net primary production
F_{po_P}	phosphorus uptake by export production
F_{po}	export production
F_{oph}	oxygenic photosynthesis
F_{dgS_M}	CH_4 production by decomposition of particulate organic matter in the surface water
F_{dgD_M}	CH_4 production by decomposition of particulate organic matter in the deep water
F_{po_C}	net removal rate of inorganic carbon from the surface ocean due to the export production
F_{dgD_C}	CO_2 production by decomposition of particulate organic matter in the deep water
F_{po_O}	net production rate of O_2 by export production
F_{dgD_O}	O_2 consumption by decomposition of particulate organic matter in the deep water
F_{dgD_P}	phosphorus recycling in the deep ocean
F_{bo}	burial of organic carbon
F_{pc}	precipitation of carbonate carbon
F_{dc}	dissolution of carbonate carbon
F_{cir_X}	net supply of net supply of dissolved component **X** to the surface ocean due to upwelling
F_{oxi_M}	CH_4 consumption by photochemical oxidation of CH_4
F_{oxi_O}	O_2 consumption by photochemical oxidation of CH_4
F_{esc_H}	hydrogen escape

To determine the variation in abundances of the gaseous and dissolved species, mass balance calculations are performed for given fluxes through particular biogeochemical processes (Tables 1 and 2). In particular, we describe below the fluxes through several biogeochemical processes, which parameterizations are originated in our model and would play key roles to determine the evolution of the surface environment after the snowball glaciation: chemical weathering of the continents (Section 2.2), phosphorus river input to the ocean (Section 2.2), biological O_2 production (Section 2.3), and a redox balance calculation (Section 2.4). For further descriptions, equations, and parameters of the model, see Supplementary Materials and Tables.

2.2. Chemical weathering of the continents and phosphorus river input

Chemical weathering of the continents is an important process in the biogeochemical cycles, because it provides cations and nutrients to the oceans and consequently stabilizes climate. We describe the global chemical weathering rates of the silicate and carbonate minerals (F_{ws} and F_{wc}, respectively) as a function of $p\mathrm{CO}_2$ and global surface temperature, T_k, as follows:

$$F_{ws} = f_a \cdot f_e \cdot f_b(p\mathrm{CO}_2, T_k) \cdot F^*_{ws} = f_w \cdot f_b(p\mathrm{CO}_2, T_k) \cdot F^*_{ws}, \quad (1)$$

$$F_{wc} = f_a \cdot f_e \cdot f_b(p\mathrm{CO}_2, T_k) \cdot F^*_{wc} = f_w \cdot f_b(p\mathrm{CO}_2, T_k) \cdot F^*_{wc}, \quad (2)$$

where F^*_{ws} and F^*_{wc} are the present-day values of chemical weathering rates of silicate and carbonate, respectively ($F^*_{ws} = 6.65 \times 10^{12}$ mol/yr and $F^*_{wc} = 13.35 \times 10^{12}$ mol/yr: Berner, 1991). The factor $f_w (= f_a \cdot f_e)$ represents the relative weathering efficiency, where f_a and f_e are the relative continental area and soil biological activity normalized by the present-day values, respectively. In the Paleoproterozoic, f_w would have been lower than that of the present-day ($f_w < 1$), because continental areas would have been smaller than that of today ($f_a < 1$), and because there were no vascular land plants ($f_e < 1$). We assume $f_a =$ 0.4–0.8 and $f_e =$ 0.1–0.25, based on the previous estimates of the evolution of continental crust (Hawkesworth and Kemp, 2006; Hawkesworth et al., 2010) and the weathering fluxes in vege-

tated and unvegetated regions (Berner, 1994; Moulton et al., 2000). We consider $f_w = 0.09$ for the nominal case and change f_w from 0.05 to 0.2 given a possible range of f_w in the Paleoproterozoic. The factor f_b represents the dependency of chemical weathering rate on both pCO_2 and surface temperature. Based on the previous weathering experiments and modeling (Tajika, 2003; Walker et al., 1981), we express f_b as follows:

$$f_b(pCO_2, T_k) = \left(\frac{pCO_2}{pCO_2^*}\right)^n \cdot \frac{\exp(-\frac{E}{RT_k})}{\exp(-\frac{E}{RT_k^*})}. \quad (3)$$

where n, E, and R represent the exponent of pCO_2 dependency, activation energy, and gas constant, respectively. We assume the values of E and n as same as those used in the previous studies (Tajika, 2003; Walker et al., 1981), i.e., $E = 15$ kcal/mol and $n = 0.3$. The terms pCO_2^* and T_k^* are the present-day atmospheric CO_2 concentration and global surface temperature respectively ($pCO_2^* = 3.15 \times 10^{-4}$ atm and $T_k^* = 285$ K, respectively). These values are obtained using the present-day solar constant and weathering efficiency ($f_w = 1$).

We consider the phosphorus riverine input (F_{rp}) to be proportional to the silicate and carbonate weathering rates (F_{ws} and F_{wc}, respectively) as follows:

$$F_{rp} = \frac{F_{ws} + F_{wc}}{F_{ws} * + F_{wc}^*} F_{rp}^*. \quad (4)$$

The term F_{rp}^* represents the phosphorus riverine input rate in the present-day ($F_{rp}^* = 0.09 \times 10^{12}$ mol/yr), which is estimated from a burial flux of phosphorus into the sediments in the steady state of our model. The contribution of P input by carbonate weathering is ~10% of total P inputs (Hartmann et al., 2014).

2.3. Biological production rate of O_2

In a long-term period, the burial rate of organic carbon corresponds to the net production rate of O_2. As described above, the burial rate of organic carbon is assumed to be proportional to the export production of organic carbon from the surface ocean to the deep ocean in out model. The export production (F_{po}) is expressed as a function of phosphorus concentration in the surface ocean ($[PO_4]_S$ in mol/L) (Yamanaka and Tajika, 1996) as follows:

$$F_{po} = R_{cp} \cdot [PO_4]_S \cdot \frac{[PO_4]_S}{[PO_4]_S + \gamma_p}, \quad (5)$$

where R_{cp} is a carbon to phosphorus ratio of organic matter, and γ_p is the half saturation constant. For R_{cp}, we simply assume that this value is same as that of the Redfield ratio ($R_{cp} = 106$). The half saturation constant γ_p is determined in order to reproduce the observations of biological productivity and phosphorus concentration in the present-day oceans ($\gamma_p = 10^{-6}$ mol/L: Paytan and McLaughlin, 2007).

The net primary production (F_{pp}) and burial rate of organic carbon (F_{bo}) are evaluated from the export production (F_{po}), assuming that they are proportional to the export production as follows:

$$F_{pp} = \frac{1}{f} \cdot F_{po}, \quad (6)$$

$$F_{bo} = \alpha \cdot F_{po} = \beta \cdot F_{pp}, \quad (7)$$

$$\beta = \alpha \cdot f, \quad (8)$$

where the parameter f is the fraction of organic matter exported from the surface ocean to the deep ocean to the net primary production, and α represents burial efficiency of organic matter into sediments.

The net primary production (F_{pp}) is taken to be a sum of oxygenic and anoxygenic photosynthesis (F_{oph} and F_{red}, respectively) as follows:

$$F_{pp} = F_{oph} + F_{red} \quad (11)$$

According to the previous redox balance model (Goldblatt et al., 2006), we consider that productivity due to anoxygenic photosynthesis is controlled by a supply of ferrous iron, as it works as an electron donor for anoxygenic photosynthesis ($Fe^{2+} + CO_2 + 11H_2O + h\nu \rightarrow 4Fe(OH)_3 + CH_2O + 8H^+$). The flux of ferrous iron in the ocean is given by the net input of reductant from mantle.

Proportions of organic matter decomposed in the surface and deep oceans are expressed as follows:

$$\text{Surface ocean: } (1 - f)F_{pp}, \quad (9)$$

$$\text{Deep ocean: } (1 - \alpha)F_{po}. \quad (10)$$

Decomposition is assumed to occur owing to aerobic respiration and/or methanogenesis, depending on O_2 concentration in the oceans. The biological production rate of O_2 due to export production (F_{po_O}) is calculated from the rates of O_2 generation via oxygenic photosynthesis (F_{oph}) and O_2 consumption through the decomposition of organic carbon in the surface oceans (see Supplementary Materials). The net production of O_2 caused by the burial of organic carbon is calculated from the biological production rate of O_2 due to export production (F_{po_O}) and the net consumption rate of O_2 (F_{dgD_O}) through organic matter decomposition in the deep ocean.

Based on the estimates of the net primary productivity and organic carbon burial rates today (Goldblatt et al., 2006), we can evaluate $\beta \sim 0.003$. Observations of the modern oceans (Eppley and Peterson, 1979) suggest that global f value is ~0.2. Thus, α would be in the order of ~0.01 in the present-day oceans. However, these values in the Proterozoic oceans are highly uncertain. In this study, we assume a fixed value of β for simplicity, and perform a sensitivity study by varying f and α (Fig. S1 and Section 2 of Supplementary Methods).

2.4. Redox balance calculations

We calculate atmospheric levels of O_2 and CH_4 from the mass balance between the input and output of both oxidants and reductants based on a redox balance model (Goldblatt et al., 2006). The model includes O_2 and CH_4 production from biosphere, hydrogen escape from the atmosphere to space, oxidative weathering of the continents, reductant input from Earth's interior, and photochemical methane oxidation in the atmosphere (see Table 1 and Supplementary Materials). The rate of hydrogen escape is limited by diffusion, which is considered as proportional to the atmospheric CH_4 concentration. The steady states of O_2 are achieved when the hydrogen escape balances the net reductant input. The model results show a bistability of O_2 levels for given net primary production and net reductant input owing to the non-linear dependency of the methane oxidation rate to the atmospheric oxygen levels derived from the results of photochemical models (Goldblatt et al., 2006). Goldblatt et al. (2006) suggest that the atmosphere–ocean system would have been in the bistable region in the Paleoproterozoic, based on estimates of the Paleoproterozoic net reductant input rate and net primary productivity. In this study, we adopt this assumption and start calculations from the low hysteresis branch of O_2 in the bistable region.

3. Results

Fig. 2 shows the evolution of surface environments after the snowball glaciation. Based on characteristic processes and

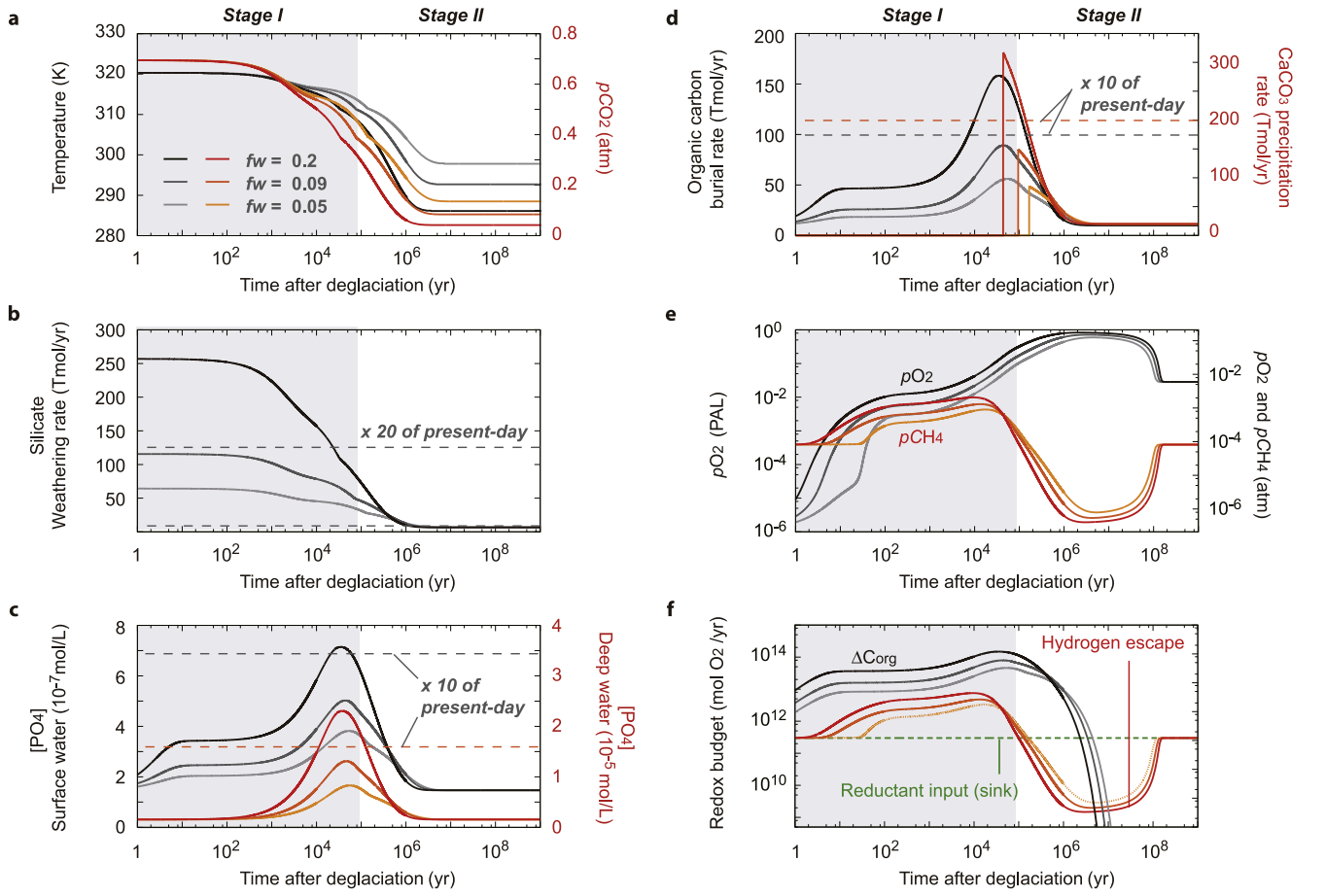

Fig. 2. Time variations in fluxes and reservoirs after the snowball glaciation. a, Surface temperatures (black) and partial pressures of CO_2 (pCO_2; red). **b,** Weathering rates of silicate rock (black). **c,** Phosphorus concentrations in the surface ocean (black) and deep ocean (red). **d,** Rates of carbonate precipitation ($CaCO_3$; red) and organic carbon burial (black). **e,** Partial pressures of atmospheric O_2 (pO_2; black) and CH_4 (pCH_4; red). **f,** Net organic carbon reservoir change, ΔC_{org} (burial rate minus weathering rate of organic carbon; black), the rate of hydrogen escape to space (red), and the input rate of reductants from the mantle (green). We assume $f_w = 0.09$ as the nominal case.

timescales, we divide a series of environmental changes into two stages (Fig. 2). Stage I ($<\sim 10^5$ yr after the termination of the snowball glaciation) is characterized by the intense chemical weathering of continents, nutrient enrichment in the oceans and a transition between oxygen steady-state levels. During this stage, carbonate precipitation is temporally inhibited because the oceans are highly undersaturated with respect to carbonate, owing to high levels of atmospheric CO_2 accumulated during the glaciation (Fig. 2d). The high levels of atmospheric CO_2 and high surface temperatures are prolonged over $\sim 10^5$ yr ($\geq$0.3 atm and $\geq$300 K, respectively) (Fig. 2a). Under transient super-greenhouse conditions, chemical weathering of the continents proceeds rapidly (Fig. 2b), and extremely high levels of the riverine input fluxes result in oceans to be highly enriched in phosphorous (5–10 times that of the present-day level) at 10^4–10^6 yr after the glaciation (Fig. 2c).

In response to the nutrient enrichments, primary production is enhanced in the oceans (Fig. 2d). As a consequence of elevated primary production followed by an elevated rate of organic carbon burial, the atmospheric O_2 level exceeds $\sim 10^{-5}$ PAL (Fig. 2e). This level is proposed as the threshold for triggering a positive feedback loop with regards to O_2; that is, when the atmospheric O_2 level reaches this level, an ozone layer forms to decrease the oxidizing efficiency of CH_4, in the atmosphere, leading to further increase in O_2 levels (Goldblatt et al., 2006). Once the positive feedback is initiated, atmospheric O_2 rapidly increases, jumping to a higher steady-state branch irreversibly (Fig. 3). The timing of this O_2 onset depends on the timescale of phosphorus accumulation in the oceans (Fig. 2d), which, in turn, is controlled by the initial atmospheric CO_2 concentration and oceanic phosphorus concentration, phosphorus cycle, and weathering efficiency. However, our sensitivity study indicates that regardless of uncertainties in these parameters, the rise of O_2 occurs within $\sim 10^4$ yr after the glaciation (Fig. 2 and Figs. S1–S4). Note that, according to Kasting (1987) and Segura et al. (2003), an ozone layer formation starts at $\sim 10^{-3}$ PAL ($\sim 10^{16}$ mol of O_2). Because the amount of a net O_2 release after deglaciation in the first 10^4 yr reaches $\sim 10^{17}$ mol of O_2, the O_2 jump should occur even for that case.

Stage II (10^5–10^8 yr after glaciation) is marked by the deposition of cap carbonate, climate stabilization, and oxygen overshoot. As a result of a supply of cations from continental weathering over $\sim 10^5$ yr, the oceans become saturated with respect to calcium carbonate (Fig. 2d). The timing of carbonate precipitation depends on initial CO_2, alkalinity, DIC, and weathering efficiency. However, regardless of such uncertainties, the carbonate precipitation always occurs after the O_2 transition (Fig. 2, Fig. S2 and Fig. S5). After the carbonate precipitation (10^5–10^6 yr), the atmospheric CO_2 levels and surface temperatures reach steady states (Figs. 2a and 2b). As a consequence of stabilization of climate, phosphorus concentrations and organic carbon burial rate in the ocean also reach steady states in $\sim 10^6$ yr (Figs. 2c and 2d).

However, even under stable conditions in climate and carbon cycles, atmospheric O_2 does not reach a final equilibrium but overshoots to $\sim$1 PAL over a period of 10^6–10^8 yr after the snowball glaciation (Fig. 2e). The accumulation of O_2 in the atmosphere is caused by the excess of net organic carbon reservoir

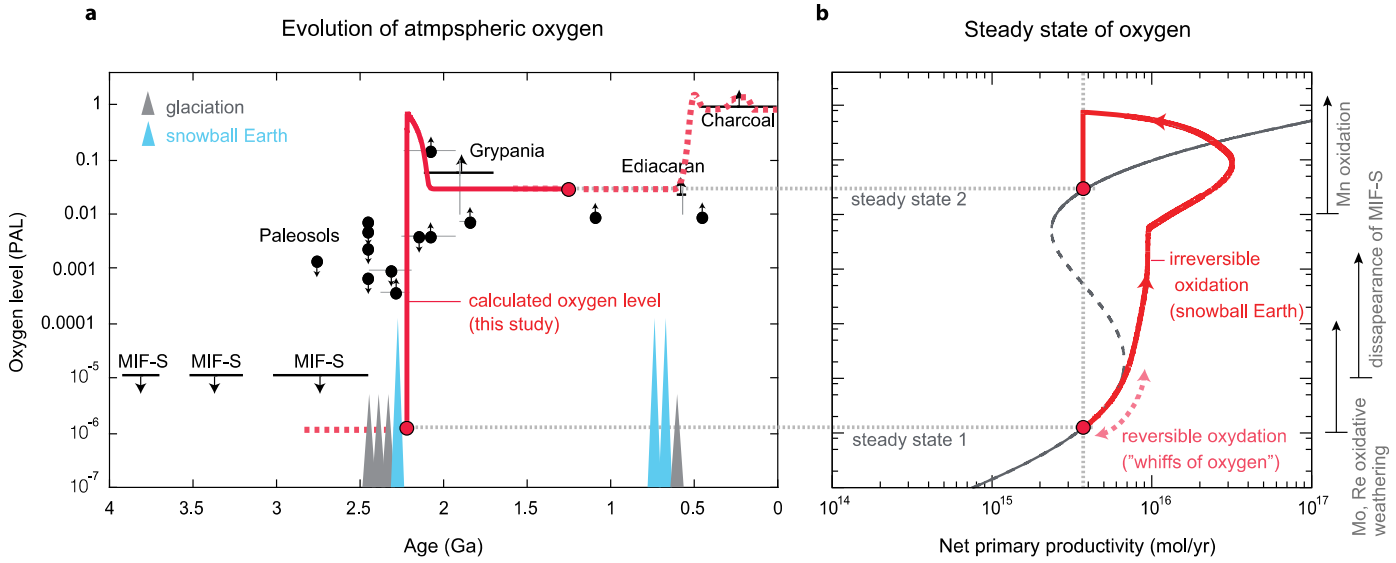

Fig. 3. Evolution of atmospheric oxygen levels. **a,** Oxygen evolution for the nominal case shown in Fig. 2 (solid red line) superimposed on a compilation of geochemical evidence for paleo-oxygen levels (Goldblatt et al., 2006 and references therein). The dashed line shows a possible evolution of oxygen levels in the Neoproterozoic. Gray dotted lines are proposed stable steady levels of oxygen. **b,** Evolutionary track of atmospheric oxygen levels after the snowball glaciation shown in Fig. 2 (red solid curve) superimposed on a bistability diagram between O_2 levels and net primary productivity given by Goldblatt et al. (2006). Solid and dashed gray curves show stable and unstable steady states, respectively. Oxygen levels constrained by proxies are also shown (Farquhar et al., 2007; Goto et al., 2013; Klemm, 2000; Pavlov and Kasting, 2002).

change relative to reductant inputs during the first 10^6 yr after the glaciation (Figs. 2d and 2f). This means that the O_2 levels during period are not equilibrated and increase unidirectionally. Under highly oxygenated conditions during this overshoot, methanogenesis is suppressed, leading to a decline in atmospheric CH_4 levels (Fig. 2e). This reduces the rate of hydrogen escape from the atmosphere to space (Fig. 2f), which results in a decrease in a net oxidation rate, or an increase in a net reduction rate, in the atmosphere–ocean system. Consequently, the accumulated O_2 is gradually consumed through the oxidation of excess reductants in the atmosphere–ocean system (e.g., reductants provided from Earth's interior) (Fig. 2e). The timescale of the overshoot is controlled by a balance between the amount of accumulated O_2 and net reduction rate. The steady-state level of ~0.01 PAL of O_2, which corresponds to a high hysteresis branch of the steady state (Goldblatt et al., 2006), is achieved $\sim 10^8$ yr after the glaciation (Fig. 3) when the rate of hydrogen escape is balanced strictly by the net reduction rate (Fig. 2f).

4. Discussion

4.1. Interpretation of geological records

Our results are in good agreement with stratigraphic evidence for surface oxygenation in the geological records. The Paleoproterozoic sedimentary rocks of the Transvaal Supergroup, South Africa, contain a low-latitude glacial diamictites (Evans et al., 1997; Kirschvink et al., 2000) which represents the Paleoproterozoic snowball glaciation (Fig. 4). In the Transvaal Supergroup, manganese–iron ore occurs between the glacial diamictites and postglacial cap carbonates (Kirschvink et al., 2000) (Fig. 4). These features are consistent with our results in which a rise of oxygen content in the atmosphere and surface ocean occurs before the deposition of cap carbonate (Fig. 2). In addition, we suggest the occurrence of an oxygen overshoot to ~1 PAL for $\sim 10^8$ yr after glaciation. This may account for the global deep-water oxygenation in 2.1 Ga (Canfield et al., 2013). The O_2 overshoot would have enhanced oxidative weathering of continental sulfides and depositions of ferric iron from the surface oceans (Bekker and Holland, 2012). The oxidative weathering of sulfides might have increased the sulfate reservoir in the oceans to levels sufficient for the precipitation of sulfate minerals. This may explain global sulfate depositions at 2.2–2.1 Ga, including sulfate evaporates found above the cap carbonate unit in the Transvaal Supergroup (Schröder et al., 2008).

Weak oxygenation of the early atmosphere and surface ocean would have pre-dated the Paleoproterozoic snowball Earth glaciation (Anbar et al., 2007; Farquhar et al., 2007; Goto et al., 2013; Kendall et al., 2010; Papineau et al., 2007). Geochemical evidence of oxidative weathering suggests an appearance of a mildly oxidizing atmosphere (10^{-8}–10^{-5} PAL) in the late Archean and Paleoproterozoic (Anbar et al., 2007; Goto et al., 2013; Kendall et al., 2010). Such 'whiffs' of oxygen may be interpreted as records of probably reversible fluctuations in O_2 levels in a low hysteresis branch, due to small changes in marine primary production (Fig. 3b and Fig. S2). Previous studies have shown that a large degree of mass-independent fractionation of sulfur isotopes (MIF-S) disappeared during repeated glaciations pre-dating the snowball event (Farquhar et al., 2007; Papineau et al., 2007). However, numerical modeling has shown that the decrease in MIF-S signatures is not only associated with a rise in O_2 but also with a collapse in atmospheric CH_4 (Zahnle et al., 2006); hence, low levels of atmospheric CH_4 at the time of deposition are an alternative interpretation for the lack of MIF-S during the repeated glaciations pre-dating the snowball glaciation (Zahnle et al., 2006). By contrast, manganese can only be oxidized by O_2 or nitric acid within marine environments (Kirschvink et al., 2000; Kopp et al., 2005), indicating that the deposition of manganese oxides within ocean settings would require large quantities of O_2 (Klemm, 2000). We suggest that the formation of manganese oxides just above the low-latitude glacial diamictites in the Transvaal Supergroup represents a distinct, irreversible O_2 transition immediately after the snowball glaciation (Fig. 3b). Large perturbations in biogeochemical cycles induced by the snowball glaciation are, thus far, the unique trigger for the GOT.

According to the recent biogeochemical study, the O_2 levels in the Mesoproterozoic would have been as low as 10^{-3} PAL (Planavsky et al., 2014). Although the present study considers $\sim 10^{-2}$ PAL as the high branch of the steady-state O_2 level, this value can vary depending on the model assumptions. For in-

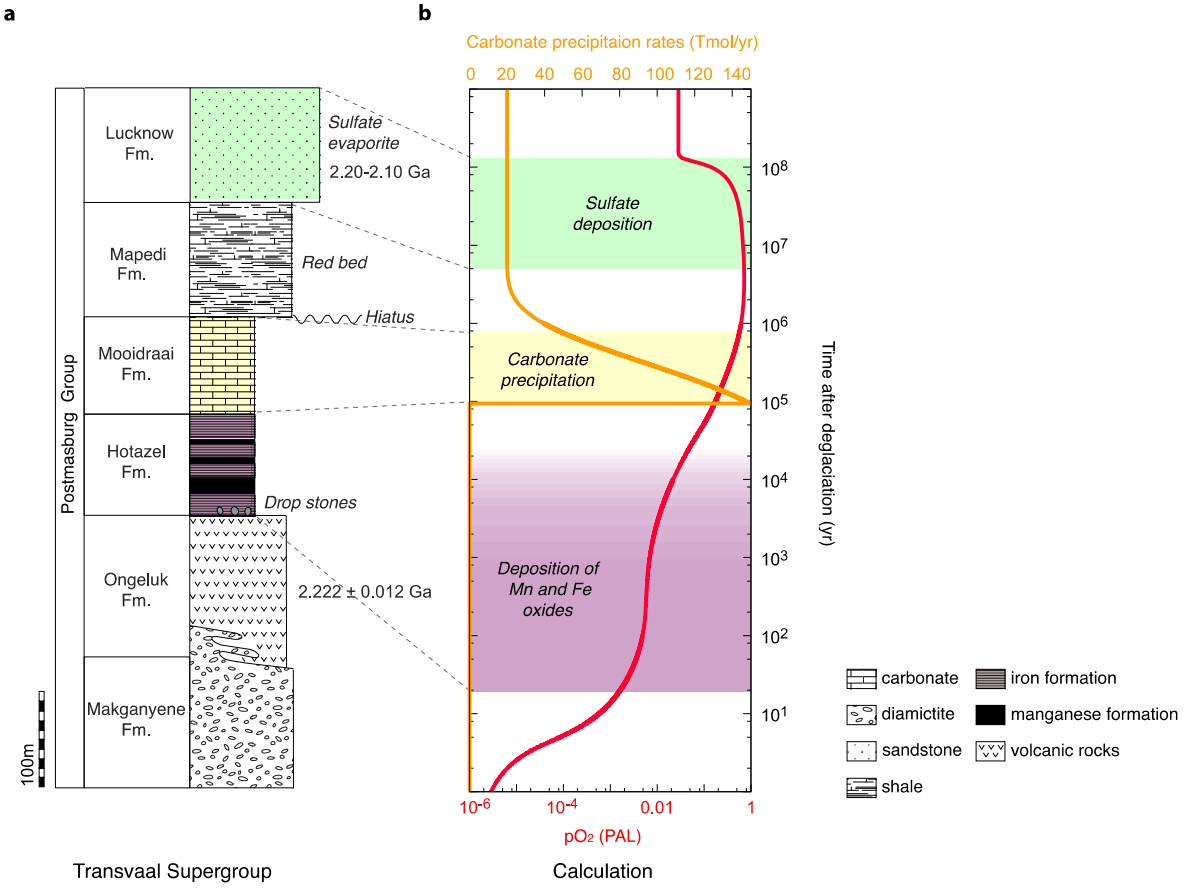

Fig. 4. Comparison of our model results with geological records. **a.** Columnar section of Transvaal Supergroup, South Africa (Kirschvink et al., 2000; Schröder et al., 2008). The Paleoproterozoic sedimentary rocks of the Transvaal Supergroup contain a low-latitude glacial diamictite (Makganeye Fm.), manganese and iron formations (Hotazel Fm.), and carbonate (Mooidraai Fm.) (Evans et al., 1997; Kirschvink et al., 2000). Red beds and molds of sulfate evaporate in Mapedi and Lucknow Fms., respectively, are formed after the formation of carbonate (Kirschvink et al., 2000; Schröder et al., 2008). Hiatus exists between Mooidraai and Mapedi formations, and the time gap due to the hiatus would be 10^7–10^8 yr or less (Schröder et al., 2008). **b.** Numerical results for the nominal case (as shown in Fig. 2). Atmospheric oxygen levels (red) and carbonate precipitation rates (yellow) are shown as a function of time after the glaciation. Our calculations show that an increase in atmospheric oxygen level precedes the precipitation of carbonate (also see Fig. 2). Long-term oxygen overshoot (>0.1 PAL over ~10^8 yr) also occurs after the carbonate formation, which may result in accumulation of sulfate ions in the oceans, followed by deposition of sulfate minerals.

stance, in our model, the steady-state O_2 level is affected by the rate of CH_4 generation in the oceans through the redox balance equations (see Goldblatt et al. (2006) and Supplementary Materials). The rate of CH_4 generation is determined by the decomposition process of organic carbon in the ocean as well as the redox state of the ocean. Although sulfate reduction plays major roles in the decomposition of organic carbon in the modern ocean, it is not considered in our model. As a result, this may overestimate the biogenic CH_4 flux in our model, and hence raise the steady-state O_2 level. Furthermore, we simply divide the ocean into two boxes, whereas multi-box models are usually used to represent the modern ocean [e.g., Ozaki et al., 2011; Ozaki and Tajika, 2013], in which the deep ocean box is oxidized by transport of O_2-rich water from high-latitude ocean box. As our two-box ocean model would tend to make the deep ocean anoxic compared with a multi-box model for the same atmospheric O_2 level, this again may overestimate the biogenic CH_4 flux and the steady-state O_2 level. In the future work, full descriptions of sulfur cycle in a multiple ocean box model would be necessary to calculate more realistic steady-state O_2 levels.

4.2. Correlation with the Lomagundi $\delta^{13}C$ excursion

The Paleoproterozoic is also marked by large positive shifts of $\delta^{13}C$ value in inorganic carbon (termed the "Lomagundi-Jutali event") deposited between ~2.2–2.1 Ga (Karhu and Holland, 1996). One interpretation of the Lomagundi event is enhanced organic carbon burial and a rise of O_2 during this period (Karhu and Holland, 1996). We show that the snowball glaciation triggers the transition of O_2 levels due to high rates of organic carbon burial, which would possibly cause a positive excursion in $\delta^{13}C$ recorded in carbonate minerals precipitated immediately after the glaciation. However, the snowball glaciation would not be able to explain the time scale of $\delta^{13}C$ excursion in the Lomagundi event (~10^8 yr) because the rate of organic carbon burial falls to a steady state (i.e., the carbon cycle reaches an equilibrium) in 10^7 yr after the glaciation in our model (Fig. 2). The timescale required to stabilize the carbon cycle could be prolonged if the chemical weathering of the continents is limited by transport of glacial tills rather than kinetics of chemical reactions (Mills et al., 2011). However, our sensitivity studies suggest that even under such transport-limited conditions for chemical weathering, the duration of enhanced organic carbon burial becomes only a few times of the nominal case (Fig. S4). One possibility to further prolong biological productivity is to take into account the positive feedback mechanism among the rise of O_2 and phosphorus input to the ocean (Bekker and Holland, 2012); that is, when O_2 rises, phosphorus input to the ocean might be enhanced due to effective weathering of apatite on the continents by oxidative weathering of sulfides, leading to prolonged, high levels of biological productivity (Bekker and Holland, 2012). Further investigations on the timescale on this feedback mechanism are required.

4.3. Implications for early life evolution

Our results show that a rapid transition (jump) from a reducing to an oxidizing atmosphere occurs $<10^4$ yr after the snowball deglaciation (Fig. 2). This timescale may be shorter than the typical timescale for the genome evolution of prokaryotes [e.g., for the rate of mutation of bacteria such as *Escherichia coli*, (Barrick et al., 2009)], implying that progressive adaptation of life to the change in redox environments reported here would have been difficult. The subsequent O_2 overshoot might have caused global oxygenation of the oceans, including deep-water environments. Thus, the abrupt and/or widespread change in redox environments could have stimulated a shift in the marine ecosystem from anaerobes to aerobes, and/or provided an environmental stress that drove biological innovations including endosymbiosis, possibly leading to the prosperity of oxygen-dependent complex life; e.g., the first fossils of the eukaryotic *Grypania sp*. and multicellular-like organisms dated at ~1.9 Ga (Payne et al., 2009) and 2.1 Ga (El Albani et al., 2010), respectively.

5. Conclusions

We evaluated the timescale and magnitudes of a rise of O_2 levels induced by the Paleoproterozoic snowball glaciation. We examined biogeochemical responses to the climate transition at the termination of the snowball glaciation using a three-box biogeochemical cycle model. During the climate recovery from the snowball glaciation, the rates of chemical weathering and nutrient input to the oceans are greatly enhanced under transient supergreenhouse conditions, which cause elevated biological productivity in the oceans. This results in both a rapid transition ($<10^4$ yr) of atmospheric O_2 from a low steady state branch ($<10^{-5}$ PAL) to a high one (~0.01 PAL or greater) and an accumulation of massive O_2 up to 1 PAL (i.e., overshoot) after the deglaciation. We show that the intense overshoot of O_2 level persists for $\sim 10^8$ yr due to slow input of reductant into the atmosphere–ocean system. These results are in good agreement with the geological records (deposition of manganese oxides and sulfate minerals, and deep-ocean oxygenation) after the Paleoproterozoic snowball glaciation. Despite an uncertainty in the interpretation of the Lomagundi event, we thus far conclude that the snowball glaciation would have been the oxidative forcing sufficient to trigger the observed dynamic transition of O_2 levels (i.e., GOT) in the Paleoproterozoic. We also speculate that early life would have been difficult to adapt to the rapid pace of change in redox states via genome evolution, possibly stimulating ecological change or biological innovation toward oxygen-dependent higher life.

Snowball Earth events cause an accumulation of CO_2, which results in a strong disequilibrium in the atmosphere–ocean system when ice melts. We show that this disequilibrium would be the driving force towards a high steady-state level of O_2. Given the occurrence of snowball Earth events at ~2.2, 0.72 and 0.64 Ga (Evans et al., 1997; Hoffman and Schrag, 2002; Kirschvink et al., 2000), phosphorus accumulations and massive releases of O_2 would have occurred at both the beginning and end of the Proterozoic (Planavsky et al., 2010; Sahoo et al., 2012) (Fig. 3). If so, snowball glaciations may have played an essential role in the phase changes of both environmental redox conditions and biological evolution during Earth's history.

Author contributions: M.H. performed calculations and wrote the manuscript. All the authors designed the study, discussed the results and commented on the manuscript. All the authors have approved the final article.

Acknowledgements

We would like to thank J.F. Kasting and C. Goldblatt for their careful and constructive comments. This study was financially supported by Grant-in-Aid for JSPS Fellows (No. 13J09134), the Program for Leading Graduate Schools, MEXT, Japan, Sasakawa Scientific Research Grant (No. 24-217), and Grant-in-Aid for Scientific Research on Innovative Areas, MEXT (No. 23103001). Y.S. thanks to Taro Maeda for discussion on biological implications.

Appendix A. Supplementary material

Supplementary material related to this article can be found online at http://dx.doi.org/10.1016/j.epsl.2015.03.005.

References

Anbar, A.D., Duan, Y., Lyons, T.W., Arnold, G.L., Kendall, B., Creaser, R., Kaufman, A.J., Gordon, G.W., Scott, C., Garvin, J., Buick, R., 2007. A whiff of oxygen before the great oxidation event? Science 317, 1903–1906. http://dx.doi.org/10.1126/science.1140325.

Barrick, J.E., Yu, D.S., Yoon, S.H., Jeong, H., Oh, T.K., Schneider, D., Lenski, R.E., Kim, J.F., 2009. Genome evolution and adaptation in a long-term experiment with *Escherichia coli*. Nature 461, 1243–1247. http://dx.doi.org/10.1038/nature08480.

Bekker, A., Holland, H.D., 2012. Oxygen overshoot and recovery during the early Paleoproterozoic. Earth Planet. Sci. Lett. 317–318, 295–304. http://dx.doi.org/10.1016/j.epsl.2011.12.012.

Berner, R.A., 1991. A model for atmospheric CO_2 over Phanerozoic time. Am. J. Sci. 291, 339–376.

Berner, R.A., 1994. Geocarb II: a revised model of atmospheric CO_2 over Phanerozoic time. Am. J. Sci. 294, 56–91.

Caldeira, K., Kasting, J.F., 1992. Susceptibility of the early Earth to irreversible glaciation caused by carbon dioxide clouds. Nature 359, 226–228.

Canfield, D.E., Ngombi-Pemba, L., Hammarlund, E.U., Bengtson, S., Chaussidon, M., Gauthier-Lafaye, F., Meunier, A., Riboulleau, A., Rollion-Bard, C., Rouxel, O., Asael, D., Pierson-Wickmann, A.-C., El Albani, A., 2013. Oxygen dynamics in the aftermath of the Great Oxidation of Earth's atmosphere. Proc. Natl. Acad. Sci. USA 110, 16736–16741. http://dx.doi.org/10.1073/pnas.1315570110.

Claire, M.W., Catling, D.C., Zahnle, K.J., 2006. Biogeochemical modelling of the rise in atmospheric oxygen. Geobiology 4, 239–269. http://dx.doi.org/10.1111/j.1472-4669.2006.00084.x.

El Albani, A., Bengtson, S., Canfield, D.E., Bekker, A., Macchiarelli, R., Mazurier, A., Hammarlund, E.U., Boulvais, P., Dupuy, J.-J., Fontaine, C., Fürsich, F.T., Gauthier-Lafaye, F., Janvier, P., Javaux, E., Ossa, F.O., Pierson-Wickmann, A.-C., Riboulleau, A., Sardini, P., Vachard, D., Whitehouse, M., Meunier, A., 2010. Large colonial organisms with coordinated growth in oxygenated environments 2.1 Gyr ago. Nature 466, 100–104. http://dx.doi.org/10.1038/nature09166.

Eppley, R., Peterson, B., 1979. Particulate organic matter flux and planktonic new production in the deep ocean. Nature 282, 677–680.

Evans, D.A., Beukes, N.J., Kirschvink, J.L., 1997. Low-latitude glaciation in the Palaeoproterozoic era. Nature 386, 262–266. http://dx.doi.org/10.1038/386262a0.

Farquhar, J., Peters, M., Johnston, D.T., Strauss, H., Masterson, A., Wiechert, U., Kaufman, A.J., 2007. Isotopic evidence for Mesoarchaean anoxia and changing atmospheric sulphur chemistry. Nature 449, 706–709. http://dx.doi.org/10.1038/nature06202.

Gaillard, F., Scaillet, B., Arndt, N.T., 2011. Atmospheric oxygenation caused by a change in volcanic degassing pressure. Nature 478, 229–232. http://dx.doi.org/10.1038/nature10460.

Goldblatt, C., Lenton, T.M., Watson, A.J., 2006. Bistability of atmospheric oxygen and the Great Oxidation. Nature 443, 683–686. http://dx.doi.org/10.1038/nature05169.

Goto, K.T., Sekine, Y., Suzuki, K., Tajika, E., Senda, R., Nozaki, T., Tada, R., Goto, K., Yamamoto, S., Maruoka, T., Ohkouchi, N., Ogawa, N.O., 2013. Redox conditions in the atmosphere and shallow-marine environments during the first Huronian deglaciation: insights from Os isotopes and redox-sensitive elements. Earth Planet. Sci. Lett. 376, 145–154. http://dx.doi.org/10.1016/j.epsl.2013.06.018.

Hartmann, J., Moosdorf, N., Lauerwald, R., Hinderer, M., West, A.J., 2014. Global chemical weathering and associated P-release — the role of lithology, temperature and soil properties. Chem. Geol. 363, 145–163. http://dx.doi.org/10.1016/j.chemgeo.2013.10.025.

Hawkesworth, C.J., Dhuime, B., Pietranik, B., Cawood, P., Kemp, I.S., Storey, C.D., 2010. The generation and evolution of the continental crust. J. Geol. Soc. Lond. 167, 229–248. http://dx.doi.org/10.1144/0016-76492009-072.

Hawkesworth, C.J., Kemp, A.I.S., 2006. Evolution of the continental crust. Nature 443, 811–817. http://dx.doi.org/10.1038/nature05191.

Hoffman, P.F., Schrag, D.P., 2002. The snowball Earth hypothesis: testing the limits of global change. Terra Nova 14, 129–155.

Jenkyns, H.C., 2010. Geochemistry of oceanic anoxic events. Geochem. Geophys. Geosyst. 11, Q03004. http://dx.doi.org/10.1029/2009GC002788.
Karhu, J., Holland, H., 1996. Carbon isotopes and the rise of atmospheric oxygen. Geology, 867–870.
Kasting, J.F., Ackerman, T.P., 1986. Climatic consequences of very high carbon dioxide levels in the Earth's early atmosphere. Science 234, 1383–1385.
Kasting, J.F., 1987. Theoretical constraints on oxygen and carbon dioxide concentrations in the Precambrian atmosphere. Precambr. Res. 34, 205–229.
Kendall, B., Reinhard, C., Lyons, T., Kaufman, A.J., Poulton, S.W., Anbar, A.D., 2010. Pervasive oxygenation along late Archaean ocean margins. Nat. Geosci. 3, 647–652. http://dx.doi.org/10.1038/ngeo942.
Kirschvink, J.L., Gaidos, E.J., Bertani, L.E., Beukes, N.J., Gutzmer, J., Maepa, L.N., Steinberger, R.E., 2000. Paleoproterozoic snowball earth: extreme climatic and geochemical global change and its biological consequences. Proc. Natl. Acad. Sci. USA 97, 1400–1405.
Klemm, D., 2000. The formation of Palaeoproterozoic banded iron formations and their associated Fe and Mn deposits, with reference to the Griqualand West deposits, South Africa. J. Afr. Earth Sci. 30, 1–24.
Kopp, R.E., Kirschvink, J.L., Hilburn, I.A., Nash, C.Z., 2005. The Paleoproterozoic snowball Earth: a climate disaster triggered by the evolution of oxygenic photosynthesis. Proc. Natl. Acad. Sci. USA 102, 11131–11136. http://dx.doi.org/10.1073/pnas.0504878102.
Lyons, T.W., Reinhard, C.T., Planavsky, N.J., 2014. The rise of oxygen in Earth's early ocean and atmosphere. Nature 506, 307–315. http://dx.doi.org/10.1038/nature13068.
Mills, B., Watson, A.J., Goldblatt, C., Boyle, R., Lenton, T.M., 2011. Timing of Neoproterozoic glaciations linked to transport-limited global weathering. Nat. Geosci. 4, 861–864. http://dx.doi.org/10.1038/ngeo1305.
Moulton, K., West, J., Berner, R., 2000. Solute flux and mineral mass balance approaches to the quantification of plant effects on silicate weathering. Am. J. Sci. 300, 539–570.
Ozaki, K., Tajima, S., Tajika, E., 2011. Conditions required for oceanic anoxia/euxinia: constraints from a one-dimensional ocean biogeochemical cycle model. Earth Planet. Sci. Lett. 304, 270–279. http://dx.doi.org/10.1016/j.epsl.2011.02.011.
Ozaki, K., Tajika, E., 2013. Biogeochemical effects of atmospheric oxygen concentration, phosphorus weathering, and sea-level stand on oceanic redox chemistry: implications for greenhouse climates. Earth Planet. Sci. Lett. 373, 129–139. http://dx.doi.org/10.1016/j.epsl.2013.04.029.
Papineau, D., Mojzsis, S.J., Schmitt, A.K., 2007. Multiple sulfur isotopes from Paleoproterozoic Huronian interglacial sediments and the rise of atmospheric oxygen. Earth Planet. Sci. Lett. 255, 188–212. http://dx.doi.org/10.1016/j.epsl.2006.12.015.
Pavlov, A., Kasting, J., 2002. Mass-independent fractionation of sulfur isotopes in Archean Sediments: strong evidence for an anoxic Archean atmosphere. Astrobiology 2, 27–41.
Payne, J.L., Boyer, A.G., Brown, J.H., Finnegan, S., Kowalewski, M., Krause, R.A., Lyons, S.K., McClain, C.R., McShea, D.W., Novack-Gottshall, P.M., Smith, F.A., Stempien, J.A., Wang, S.C., 2009. Two-phase increase in the maximum size of life over 3.5 billion years reflects biological innovation and environmental opportunity. Proc. Natl. Acad. Sci. USA 106, 24–27. http://dx.doi.org/10.1073/pnas.0806314106.
Paytan, A., McLaughlin, K., 2007. The oceanic phosphorus cycle. Chem. Rev. 107, 563–576. http://dx.doi.org/10.1021/cr0503613.
Planavsky, N.J., Rouxel, O.J., Bekker, A., Lalonde, S.V., Konhauser, K.O., Reinhard, C.T., Lyons, T.W., 2010. The evolution of the marine phosphate reservoir. Nature 467, 1088–1090. http://dx.doi.org/10.1038/nature09485.
Planavsky, N.J., Reinhard, C.T., Wang, X., McGoldrick, P., Rainbird, R.H., Johnson, T., Fisher, W.W., Lyons, T.W., 2014. Low-Mid-Proterozoic atmospheric oxygen levels and the delayed rise of animals. Science 346, 635–638.
Rye, R., Holland, H.D., 1998. Paleosols and the evolution of atmospheric oxygen: a critical review. Am. J. Sci. 298, 621–672.
Sahoo, S.K., Planavsky, N.J., Kendall, B., Wang, X., Shi, X., Scott, C., Anbar, A.D., Lyons, T.W., Jiang, G., 2012. Ocean oxygenation in the wake of the Marinoan glaciation. Nature 489, 546–549. http://dx.doi.org/10.1038/nature11445.
Schröder, S., Bekker, a., Beukes, N.J., Strauss, H., van Niekerk, H.S., 2008. Rise in seawater sulphate concentration associated with the Paleoproterozoic positive carbon isotope excursion: evidence from sulphate evaporites in the ~2.2–2.1 Gyr shallow-marine Lucknow Formation, South Africa. Terra Nova 20, 108–117. http://dx.doi.org/10.1111/j.1365-3121.2008.00795.x.
Segura, A., Krelove, K., Kasting, J.F., Sommerlatt, D., Meadows, V., Crisp, D., Cohen, M., Mlawer, E., 2003. Ozone concentrations and ultraviolet fluxes on Earth-like planets around other stars. Astrobiology 3, 689–708.
Tajika, E., 2003. Faint young Sun and the carbon cycle: implication for the Proterozoic global glaciations. Earth Planet. Sci. Lett. 214, 443–453. http://dx.doi.org/10.1016/S0012-821X(03)00396-0.
Walker, J.C.G., Hays, P.B., Kasting, J.F., 1981. A negative feedback mechanism for the long-term stabilization of Earth's surface temperature. J. Geophys. Res. 86, 9776–9782. http://dx.doi.org/10.1029/JC086iC10p09776.
Yamanaka, Y., Tajika, E., 1996. The role of the vertical fluxes of particulate organic matter and calcite in the oceanic carbon cycle: studies using an ocean biogeochemical general circulation model. Glob. Biogeochem. Cycles 10, 361–382.
Zahnle, K., Claire, M.W., Catling, D.C., 2006. The loss of mass-independent fractionation in sulfur due to a Palaeoproterozoic collapse of atmospheric methane. Geobiology 4, 271–283. http://dx.doi.org/10.1111/j.1472-4669.2006.00085.x.